

**FUNCTIONAL CELLULOSE NANOCRYSTAL-
ALGINATE HYDROGEL BEADS PREPARED
FROM OIL PALM FRONDS FOR THE
ADSORPTION OF 4-CHLOROPHENOL IN
AQUEOUS SOLUTION**

TUAN SHERWYN HAMIDON

UNIVERSITI SAINS MALAYSIA

2023

**FUNCTIONAL CELLULOSE NANOCRYSTAL-
ALGINATE HYDROGEL BEADS PREPARED
FROM OIL PALM FRONDS FOR THE
ADSORPTION OF 4-CHLOROPHENOL IN
AQUEOUS SOLUTION**

by

TUAN SHERWYN HAMIDON

**Thesis submitted in fulfilment of the requirements
for the degree of
Doctor of Philosophy**

January 2023

ACKNOWLEDGEMENT

In the name of Allah, the Most Gracious and the Most Merciful

First and foremost, I praise Almighty Allah for providing me with this opportunity and granting me the strength, courage, and capability to complete my research study successfully would like to thank and express my sincere indebtedness to my supervisor, Assoc. Prof. Dr. Mohd. Hazwan Hussin who had been an inspiration throughout my research work. He consistently allowed this research to be my work but allowed to think critically about the basis of the research study and steered me in the right direction whenever he thought I needed it. I would also like to sincerely acknowledge my co-supervisors Prof. Rohana Adnan and Assoc. Prof. M. K. Mohamad Haafiz, for their continuous guidance, keenness, dedication, and patience extended to me during the research period. I would like to sincerely acknowledge the financial support offered by Universiti Sains Malaysia through Research University Incentive, RUI grant (1001/PKIMIA/8011077) and USM External Grant (304/PKIMIA/6501094/I129). Million thanks and gratitude to all the administrative and technical staff, especially laboratory assistants and science officers at the School of Chemical Sciences and School of Archaeology, for their invaluable advice and assistance throughout the project. Not to forget, I humbly extend my most profound appreciation to all the lecturers under whom I had the blessing to gain knowledge and to all my lab mates for their unconditional support, motivation, and prayers extended to me throughout. Finally, I must express my profound gratitude to my parents and siblings for providing unfailing support, moral boost, and continuous encouragement throughout my years of study and through researching and writing this thesis. This accomplishment would not have been possible without them. Thank you.

TABLE OF CONTENTS

ACKNOWLEDGEMENT	ii
TABLE OF CONTENTS	iii
LIST OF TABLES	x
LIST OF FIGURES	xiii
LIST OF ABBREVIATIONS	xxi
LIST OF SYMBOLS	xxiv
ABSTRAK	xxvii
ABSTRACT	xxix
CHAPTER 1 INTRODUCTION	1
1.1 Research background	1
1.2 Problem statement	4
1.3 Research objectives	6
1.4 Scope of study	6
1.5 Gap of knowledge	8
1.6 Thesis outline	8
CHAPTER 2 LITERATURE REVIEW	10
2.1 Oil palm biomass.....	10
2.2 Overview of nanocellulose.....	14
2.3 Cellulose nanocrystals.....	18
2.4 Characterization and properties of cellulose nanocrystals	25
2.5 Surface modification of cellulose nanocrystals.....	29
2.6 Wastewater remediation using cellulose-based beads	34
2.6.1 Overview of wastewater treatment.....	34
2.6.2 Overview of cellulose-based beads	37
2.6.2(a) Hydrogels.....	39

2.6.2(b)	Aerogels.....	40
2.6.3	Preparation of cellulose-based beads	41
2.6.4	Properties and characteristics of nanocellulose-based hydrogel beads.....	47
2.7	Adsorption process	51
2.7.1	Adsorption isotherm modelling.....	54
2.7.1(a)	Langmuir adsorption isotherm model.....	54
2.7.1(b)	Freundlich adsorption isotherm model.....	56
2.7.1(c)	Temkin adsorption isotherm model.....	57
2.7.1(d)	Dubinin-Radushkevich adsorption isotherm model	57
2.7.2	Kinetic models	60
CHAPTER 3	EXPERIMENTAL	62
3.1	Overview of the experimental procedure	62
3.2	Raw material and chemical reagents	64
3.3	Equipment and instrumentation	66
3.4	Preparation of powdered OPF and pretreatment process	68
3.5	Extraction protocol to produce cellulose nanocrystals (CNC-OPF)	69
3.5.1	Alkali treatment.....	71
3.5.2	Bleaching	71
3.5.3	Acid hydrolysis treatment	71
3.6	Characterization of isolated cellulose nanocrystals	72
3.6.1	Attenuated Total Reflectance Fourier Transform Infrared (ATR-FTIR) Spectroscopy	73
3.6.2	Cross-Polarization Magic-Angle Spinning ¹³ C solid-state Nuclear Magnetic Resonance (CP/MAS ¹³ C NMR) Spectroscopy	73
3.6.3	Thermogravimetric Analysis (TGA).....	73
3.6.4	Differential Scanning Calorimetry (DSC)	74

3.6.5	X-ray Diffraction (XRD) analysis.....	74
3.6.6	Scanning Electron Microscopy (SEM)	75
3.6.7	Transmission Electron Microscopy (TEM)	75
3.6.8	Nitrogen adsorption-desorption measurements	76
3.7	Functionalization of cellulose nanocrystal/alginate hydrogel beads.....	76
3.7.1	Preparation of cellulose nanocrystal/alginate hydrogel	77
3.7.2	Preparation of porous CTAC-cellulose nanocrystal/alginate	79
	hydrogel beads	
3.7.2(a)	Modification of CNC-OPF with cetyltrimethylammonium chloride	79
3.7.2(b)	Enhancing the porosity of CTAC modified-cellulose nanocrystal/alginate hydrogel beads.....	79
3.7.3	Preparation of porous Cu modified-cellulose nanocrystal/alginate hydrogel beads	80
3.8	Measurement of adsorption performance.....	81
3.8.1	Influence of various parameters on 4-chlorophenol adsorption.....	82
3.8.1(a)	Effect of contact time	82
3.8.1(b)	Effect of crosslinking time	82
3.8.1(c)	Effect of adsorbent dosage	83
3.8.1(d)	Effect of initial 4-chlorophenol concentration.....	83
3.8.1(e)	Effect of stirring speed	83
3.8.1(f)	Effect of hydrogel bead size	84
3.8.1(g)	Effect of medium pH	84
3.8.2	Adsorption isotherm modelling	84
3.8.3	Effect of temperature and thermodynamic study	85
3.8.4	Adsorption kinetics	85
3.8.5	Applicability of the adsorption isotherm and kinetic models	86

3.9	Characterization of surface modified and unmodified cellulose nanocrystal/alginate hydrogel beads	87
3.9.1	ATR-FTIR spectroscopy	87
3.9.2	Thermalgravimetric (TGA) analysis	87
3.9.3	SEM-EDX analysis	88
3.9.4	Nitrogen adsorption-desorption measurements	89
3.9.5	X-ray photoelectron spectroscopy	89
3.9.6	The pH point zero charge (pH _{pzc}).....	90
3.9.7	Zeta potential analysis.....	90
3.9.8	Determination of water content, swelling behaviour and porosity ..	90
3.10	Regeneration and reusability study	91
CHAPTER 4 RESULTS AND DISCUSSION.....		93
4.1	Analysis of oil palm frond composition.....	93
4.2	Characterization of isolated cellulose nanocrystals (CNC-OPF).....	94
4.2.1	Fourier transform infrared spectroscopy (FTIR)	94
4.2.2	CP/MAS ¹³ C NMR spectroscopy.....	98
4.2.3	Thermogravimetric analysis (TGA).....	101
4.2.4	Differential Scanning Calorimetry (DSC)	106
4.2.5	X-ray Diffraction (XRD) analysis.....	108
4.2.6	Scanning Electron Microscopy (SEM)	113
4.2.7	Transmission Electron Microscopy (TEM)	115
4.2.8	BET surface area and porosity	117
4.3	Application of cellulose nanocrystal-alginate (CNC-ALG) hydrogel beads.....	121
4.3.1	Preparation of CNC-ALG hydrogel beads.....	121
4.3.2	Effect of experimental conditions on 4-chlorophenol adsorption..	123
	4.3.2(a) Effect of contact time and optimum dosage	123

4.3.2(b)	Effect of initial 4-chlorophenol concentration and solution temperature	125
4.3.2(c)	Effect of crosslinker concentration, crosslinking time and hydrogel bead size	127
4.3.2(d)	Effect of solution pH	130
4.3.3.	Adsorption equilibrium isotherms	131
4.3.4.	Adsorption thermodynamics	136
4.3.5.	Adsorption rate.....	139
4.3.6.	Mechanism of 4-chlorophenol adsorption	143
4.3.6(a)	Intraparticle-diffusion model.....	143
4.3.6(b)	EDX analysis	145
4.3.7.	Characterization of CNC-ALG hydrogel beads.....	146
4.3.7(a)	FTIR spectroscopy.....	150
4.3.7(b)	Thermal behaviour.....	151
4.3.7(c)	Textural characterization	153
4.3.7(d)	Determination of point of zero charge (pHpzc) and zeta potential.....	154
4.4.	Application of cetyltrimethylammonium chloride-modified cellulose nanocrystal/alginate hydrogel beads (CTAC-CNC/ALG) hydrogel beads.....	155
4.4.1.	Optimal composition of CTAC-CNC/ALG hydrogel beads.....	155
4.4.2.	Influence of various parameters on 4-chlorophenol adsorption.....	158
4.4.2(a)	Effect of contact time and optimum dosage	159
4.4.2(b)	Effect of initial 4-chlorophenol concentration.....	161
4.4.2(c)	Optimization of crosslinking time, agitation speed and hydrogel bead size	162
4.4.2(d)	Effect of medium pH	166
4.4.3	Adsorption equilibrium isotherm modelling.....	168

4.4.4	Effect of temperature and thermodynamic study	176
4.4.5	Adsorption kinetics	181
4.4.6	Mechanism analysis of 4-chlorophenol adsorption.....	190
4.4.6(a)	Intraparticle-diffusion model.....	190
4.4.6(b)	EDX analysis	195
4.4.6(c)	XPS analysis	197
4.4.7	Characterization of porous CTAC-CNC/ALG hydrogel beads	202
4.4.7(a)	FTIR spectroscopy.....	202
4.4.7(b)	Thermal behaviour.....	205
4.4.7(c)	Textural characterization	207
4.4.7(d)	Determination of point of zero charge (pH _{PZC})	211
4.4.7(e)	Zeta potential measurement.....	212
4.5.	Application of copper-modified cellulose nanocrystal/alginate (Cu-CNC/ALG) hydrogel beads	214
4.5.1.	Optimization of copper-modified CNC and ALG loading	214
4.5.2.	Effect of various operating parameters on 4-chlorophenol	
	adsorption.....	216
4.5.2(a)	Effect of contact time and adsorbent dosage.....	216
4.5.2(b)	Effect of ionic strength	218
4.5.2(c)	Effect of initial concentration of 4-chlorophenol solution	220
4.5.2(d)	Effect of solution pH	222
4.5.3.	Adsorption isotherm modelling	223
4.5.4.	Effect of solution temperature and evaluation of thermodynamic parameters	229
4.5.5.	Adsorption kinetics	232
4.5.6	Mechanism of 4-chlorophenol adsorption	241
4.5.7	Characterization of Cu-CNC/ALG hydrogel beads	247

4.5.7(b)	Textural characterization.....	249
4.5.7(c)	Point of zero charge (pH _{PZC}) and zeta potential analyses.....	251
4.6	Regeneration and reusability performance.....	253
4.7	Performance evaluation compared to other adsorbents.....	255
CHAPTER 5 CONCLUSION AND RECOMMENDATIONS		260
5.1.	Conclusion.....	260
5.2.	Recommendations	264
REFERENCES.....		268
APPENDICES		
LIST OF PUBLICATIONS		

LIST OF TABLES

	Page
Table 2.1	Lignocellulosic composition and extractives content of oil palm fronds based on previous research studies 13
Table 2.2	Primary isolation methods/treatments of cellulose pulp-derived nanocellulose 17
Table 2.3	Effect of isolation method and adopted conditions on the characteristics of CNCs based on recent studies 20
Table 2.4	Previous studies on surface modification of nanocellulose substrates along with their salient features and applications 33
Table 2.5	Characteristics and properties of numerous nanocellulose-based hydrogel beads reported in the literature 50
Table 2.6	Most widely adopted equilibrium adsorption isotherm models for cellulose-based beads..... 59
Table 3.1	List of reagents and chemicals 65
Table 3.2	Physical and chemical properties of 4-chlorophenol 66
Table 3.3	List and description of instruments and equipment used..... 67
Table 4.1	Proximate analysis of raw and pretreated OPF biomass..... 93
Table 4.2	The summary of the FTIR absorption bands and their corresponding assignments for α -cellulose and CNC-OPF 97
Table 4.3	Comparison of thermal degradation profiles of α -cellulose and CNC-OPF with literature 105
Table 4.4	Comparison of crystallinity index of CNC based on different sources and calculation methods..... 110
Table 4.5	Specific surface area and porosity characteristics of α -cellulose and CNC-OPF 120
Table 4.6	Adsorption isotherm parameters for the adsorptive uptake of 4-CP onto CNC-ALG hydrogel beads at 30, 40 and 50 °C 134
Table 4.7	Thermodynamic parameters related to the adsorption of 4-CP onto CNC-ALG hydrogel beads 138

Table 4.8	Kinetic constant parameters and determination coefficients for 4-CP adsorption by CNC-ALG hydrogel beads using the linear regression method at 30 °C	142
Table 4.9	Intra-particle model rate parameters for various initial 4-CP concentrations at 30 °C	144
Table 4.10	Diameter of CNC-ALG hydrogel beads obtained by analyzing digital images	148
Table 4.11	Specific surface area and porosity characteristics of CNC, pure alginate beads and CNC-alginate hydrogel beads	154
Table 4.12	Isotherm model parameters for 4-CP adsorption by CTAC-CNC/ALG hydrogel beads using the linear regression method	174
Table 4.13	R_L values for the adsorption of 4-CP onto CTAC-CNC/ALG hydrogel beads based on Langmuir isotherm (type 1) model.....	176
Table 4.14	Thermodynamic parameters concerning the adsorption of 4-CP by porous CTAC-CNC/ALG hydrogel beads.....	180
Table 4.15	Parameters and determination coefficients for 4-CP adsorption by CTAC-CNC/ALG hydrogel beads based on non-linear forms of pseudo-first-order and pseudo-second-order kinetics.....	183
Table 4.16	Kinetic constant parameters and determination coefficients for 4-CP adsorption by CTAC-CNC/ALG hydrogel beads using the linear regression method at 30 °C	185
Table 4.17	Intra-particle model rate parameters for various initial 4-CP concentrations at 30 °C	194
Table 4.18	Specific surface area and porosity characteristics of CNC, pure alginate beads and CTAC-CNC/ALG hydrogel beads.....	209
Table 4.19	Isotherm model parameters for 4-CP adsorption by Cu-CNC/ALG hydrogel beads using the linear and non-linear regression method....	227
Table 4.20	R_L values concerning the adsorption of 4-CP onto Cu-CNC/ALG hydrogel beads based on Langmuir-1 isotherm.....	228
Table 4.21	Thermodynamic parameters relating to the adsorption of 4-CP onto Cu-CNC/ALG hydrogel beads.....	231
Table 4.22	Parameters and determination coefficients for 4-CP adsorption by Cu-CNC/ALG hydrogel beads based on non-linear forms of pseudo-first-order and pseudo-second-order kinetics.....	234

Table 4.23	Kinetic constant parameters and determination coefficients for 4-CP adsorption onto Cu-CNC/ALG hydrogel beads using the linear regression method at 30 °C	236
Table 4.24	Intra-particle model rate parameters for various initial 4-CP concentrations at 30 °C with regards to Cu-CNC/ALG hydrogel beads	243
Table 4.25	Specific surface area and porosity characteristics of CNC, pure alginate beads and Cu-CNC/ALG hydrogel beads	251
Table 4.26	Comparison of various adsorbents utilized for the adsorptive removal of 4-CP from aqueous media	257

LIST OF FIGURES

	Page
Figure 2.1 Major oil palm biomass residues	11
Figure 2.2 Availability of major oil palm biomass residues in Malaysia in 2017	12
Figure 2.3 a) Chemical structure and b) microstructure of cellulose	16
Figure 2.4 Schematic representation of a pretreatment process applied on lignocellulosic biomass	19
Figure 2.5 The mechanism of chemical and mechanical methods for producing CNC and CNF from cellulose	23
Figure 2.6 Schematic representation of the most commonly used surface modification routes of nanocellulose	32
Figure 2.7 Number of annual publications on wastewater treatment employing cellulosic adsorbents (Database: Scopus; search (title, abstract, keywords): cellulose for wastewater treatment; Year: 2012-2022)	36
Figure 2.8 Schematic of methods for formation of two types of ionic hydrogels. An example of a ‘polyanion’ is sodium alginate and an example of an ‘ionotropic’ hydrogel is calcium alginate	39
Figure 2.9 Depiction of (a) external ionotropic gelation and (b) internal ionotropic gelation/emulsification processes	42
Figure 2.10 Schematic showing the external and internal structure of the bead.....	45
Figure 2.11 Schematic representation of the electrostatic interaction between chemical crosslinker Ca^{2+} ions and COO^- groups of alginate	46
Figure 2.12 Illustrative representation of the three successive steps of an adsorption process indicating mass transfer	51
Figure 2.13 The Brunauer classification of adsorption isotherms for a solid-liquid system.....	53
Figure 3.1 Flowchart diagram of the experimental work.....	63
Figure 3.2 Oil palm plantation in Nibong Tebal, Pulau Pinang	64
Figure 3.3 Schematic illustration depicting the isolation of CNC from OPF	70
Figure 3.4 A schematic route of the fabrication process of CNC-ALG hydrogel beads	78

Figure 4.1	FTIR spectra of raw OPF fiber, α -cellulose and CNC-OPF.....	95
Figure 4.2	Chemical structure of native cellulose.....	96
Figure 4.3	Solid-state ^{13}C NMR spectra of (a) α -cellulose and (b) CNC-OPF....	100
Figure 4.4	(a) TG and (b) DTG thermograms pertaining to the decomposition of α -cellulose and CNC-OPF	103
Figure 4.5	DSC thermograms of α -cellulose and CNC-OPF.....	107
Figure 4.6	(a) X-ray diffractograms of raw OPF fiber, α -cellulose and CNC-OPF, and (b) X-ray diffraction pattern of CNC-OPF depicting the deconvolution of major amorphous and crystalline domains	109
Figure 4.7	SEM micrographs of (a) α -cellulose and (b) CNC-OPF acquired at a magnification of $500\times$	114
Figure 4.8	TEM micrographs of CNC-OPF acquired at $12,500\times$ magnification (scale bar = 500 nm)	116
Figure 4.9	N_2 adsorption and desorption isotherms of (a) α -cellulose and (b) CNC-OPF obtained at 77 K	118
Figure 4.10	(a) 4-CP removal (%) of 2 wt.% of ALG containing hydrogel beads with varying wt.% of CNCs (concentration of 4-CP solution = 100 mg L^{-1} , volume of 4-CP solution = 100 mL, dosage of hydrogel beads = 3.0 g). (b) 4-CP removal (%) of 2 wt.% CNC containing hydrogel beads with varying wt.% of ALG.....	122
Figure 4.11	Effect of (a) contact time (dosage = 2 g/100 mL; $C_0 = 100\text{ mg L}^{-1}$) and (b) adsorbent dosage ($T = 303\text{ K}$; contact time = 6 h; $C_0 = 100\text{ mg L}^{-1}$) on the 4-CP adsorption characteristics of CNC-ALG hydrogel beads	124
Figure 4.12	(a) Removal of 4-CP versus initial concentration (dosage = 3 g/100 mL; $T = 303\text{ K}$) and (b) effect of solution temperature on the removal of 4-CP ($C_0 = 100\text{ mg L}^{-1}$; dosage = 3 g/100 mL)	126
Figure 4.13	Effect of (a) crosslinker concentration ($T = 303\text{ K}$; gelation time = 1 h), (b) crosslinking time (dosage = 2 g/100 mL; $C_0 = 100\text{ mg L}^{-1}$) and (c) hydrogel bead size ($T = 303\text{ K}$; contact time = 4 h; $C_0 = 100\text{ mg L}^{-1}$) on the 4-CP adsorption characteristics of CNC-ALG hydrogel beads	128
Figure 4.14	Effect of solution pH on 4-CP removal performance ($T = 303\text{ K}$; contact time = 6 h; dosage = 3 g/100 mL; $C_0 = 100\text{ mg L}^{-1}$).....	130

Figure 4.15	Linearized (a) Langmuir-1, (b) Freundlich and (c) Temkin isotherm plots representing the adsorption of 4-CP onto CNC-ALG hydrogel beads (Conditions: $C_o = 100 \text{ mg L}^{-1}$; volume = 100 mL; adsorbent dosage = 3.0 g; contact time = 6 h; pH = 2)	132
Figure 4.16	Van't Hoff plot of $\ln K_o$ against $1/T$ for 4-CP adsorption onto CNC-ALG hydrogel beads	137
Figure 4.17	(a) Plot of q_t versus time for various 4-CP concentrations and (b) pseudo-second-order kinetic model fitting for batch adsorption of 4-CP of various initial 4-CP concentrations on CNC-ALG hydrogel beads (Conditions: sorbent dosage = 3.0 g; $T = 30 \text{ }^\circ\text{C}$; pH = 2).....	140
Figure 4.18	(a) Pseudo-first-order and (b) Elovich plots for batch adsorption of 100 mg L^{-1} 4-CP solution onto CNC-ALG hydrogel beads (Conditions: sorbent dosage = 3.0 g; $T = 30 \text{ }^\circ\text{C}$; pH = 2).....	141
Figure 4.19	Weber-Morris plots for batch adsorption of 4-CP solution onto CNC-ALG hydrogel beads with regards to varying initial 4-CP concentration at $30 \text{ }^\circ\text{C}$	143
Figure 4.20	EDX analysis for CNC-ALG hydrogel beads (a) before and (b) after 4-CP adsorption	145
Figure 4.21	Proposed mechanism of adsorption depicting the interaction forces between CNC-ALG hydrogel beads with 4-CP.....	146
Figure 4.22	(a) Magnified digital micrographs of pure ALG hydrogel beads, (b) CNC-ALG hydrogel beads before 4-CP adsorption (10 \times magnification), (c) CNC-ALG hydrogel beads after 4-CP adsorption (50 \times magnification), and (d) digital photograph depicting the outlook of CNC-ALG hydrogel beads	147
Figure 4.23	(a) Comparison of water content and porosity of CNC-ALG and pure ALG hydrogel beads and (b) swelling ratio of CNC-ALG and pure ALG hydrogel beads	149
Figure 4.24	FT-IR spectra of sodium alginate (SA) powder, pure alginate (ALG) hydrogel beads and CNC-ALG hydrogel beads	151
Figure 4.25	TG and DTG plots of CNC-ALG hydrogel beads and CNC.....	152
Figure 4.26	(a) Surface morphology of CNC-ALG hydrogel beads (100 \times magnification) and (b) its cross-section (10,000 \times magnification).....	153

Figure 4.27	Point of zero charge (pH_{PZC}) of CNC-ALG hydrogel beads in 0.05 M NaCl	155
Figure 4.28	(a) 4-CP removal (%) of 2 wt.% of ALG containing hydrogel beads with varying wt.% of CNCs (concentration of 4-CP solution = 100 mg L^{-1} , volume of 4-CP solution = 100 mL, dosage of hydrogel beads = 0.5 g). (b) 4-CP removal (%) of 2 wt.% CNC containing hydrogel beads with varying wt.% of ALG	156
Figure 4.29	The surface modification scheme of CNC-OPF by CTAC cationic surfactant	157
Figure 4.30	TEM images of the resulting (a) CTAC-CNC and (b) unmodified CNC (obtained at 500 nm).....	158
Figure 4.31	Influence of (a) contact time and (b) adsorbent dosage on the 4-CP adsorption characteristics by porous CTAC-CNC/ALG hydrogel beads	160
Figure 4.32	Influence of initial 4-CP concentration on its adsorption characteristics by porous CTAC-CNC/ALG hydrogel beads.....	162
Figure 4.33	Influence of crosslinking on 4-CP adsorption characteristics by porous CTAC-CNC/ALG hydrogel beads.....	163
Figure 4.34	Influence of (a) agitation speed and (b) hydrogel bead size on 4-CP adsorption characteristics by porous CTAC-CNC/ALG hydrogel beads	165
Figure 4.35	Influence of medium pH on 4-CP adsorption characteristics by porous CTAC-CNC/ALG hydrogel beads.....	167
Figure 4.36	(a) Non-linear and (b) linear Langmuir isotherm, (c) non-linear and (d) linear Freundlich isotherm, (e) Temkin and (f) Dubinin-Radushkevich isotherm plots representing the adsorption of 4-CP onto CTAC-CNC/ALG hydrogel beads	173
Figure 4.37	(a) Effect of temperature on the adsorption of 4-CP onto CTAC-CNC/ALG hydrogel beads (Conditions: $\text{pH} = 7$, adsorbent dose = 1.0 g, initial 4-CP concentration = 100 mg L^{-1} ; contact time = 3 h), and (b) van't Hoff plot of $\ln K_o$ against $1/T$ for 4-CP adsorption onto CTAC-CNC/ALG hydrogel beads	178

Figure 4.38	Non-linear pseudo-first-order and pseudo-second-order kinetic models fitting for batch adsorption of 4-CP with varying initial 4-CP concentrations by CTAC-CNC/ALG hydrogel beads	182
Figure 4.39	(a) Plot of q_t vs. time for various 4-CP concentrations and (b) pseudo-second-order (model I) kinetic model fitting for batch adsorption of 4-CP under various initial 4-CP concentrations on CTAC-CNC/ALG hydrogel beads.....	184
Figure 4.40	(a) Pseudo-first-order and (b) Elovich plots for batch adsorption of 100 mg L ⁻¹ 4-CP solution onto CTAC-CNC/ALG hydrogel beads....	186
Figure 4.41	Plot of $\ln (q_e - q_t)$ versus time (t) (pseudo-first-order) for (a) 50 mg L ⁻¹ , (b) 200 mg L ⁻¹ , (c) 400 mg L ⁻¹ , (d) 600 mg L ⁻¹ , (e) 800 mg L ⁻¹ and (e) 1000 mg L ⁻¹ initial 4-CP concentration at 30 °C	187
Figure 4.42	Pseudo-second-order (model II) kinetic model fitting for batch adsorption of 4-CP of various initial 4-CP concentrations on CTAC-CNC/ALG hydrogel beads.....	188
Figure 4.43	Plot of q_t versus $\ln (t)$ (Elovich isotherm) for (a) 50 mg L ⁻¹ , (b) 200 mg L ⁻¹ , (c) 400 mg L ⁻¹ , (d) 600 mg L ⁻¹ , (e) 800 mg L ⁻¹ and (e) 1000 mg L ⁻¹ initial 4-CP concentration at 30 °C	189
Figure 4.44	(a) Weber-Morris plots for batch adsorption of 100 mg L ⁻¹ 4-CP solution onto CTAC-CNC/ALG hydrogel beads and (b) plot of $\log k_{id}$ against \log (initial 4-CP concentration).....	192
Figure 4.45	Plot of q_t versus $t^{0.5}$ (Weber-Morris plot) for (a) 50 mg L ⁻¹ , (b) 200 mg L ⁻¹ , (c) 400 mg L ⁻¹ , (d) 600 mg L ⁻¹ , (e) 800 mg L ⁻¹ and (e) 1000 mg L ⁻¹ initial 4-CP concentration at 30 °C	193
Figure 4.46	EDX analysis for CTAC-CNC/ALG hydrogel beads (a) before and (b) after 4-CP adsorption.....	196
Figure 4.47	The XPS analysis of CTAC-CNC/ALG hydrogel beads before and after 4-CP adsorption with (a) wide-scan spectra and high-resolution spectra of; (b) Ca 2p, (c) C 1s, (d) O 1s and (e) N 1s	198
Figure 4.48	Proposed mechanism of adsorption depicting the interaction forces between CTAC-CNC/ALG hydrogel beads with 4-CP	201

Figure 4.49	FT-IR spectra of (a) unmodified CNC, CTAC and CTAC-CNC and (b) CTAC-CNC/ALG hydrogel beads before adsorption and 4-CP loaded CTAC-CNC/ALG hydrogel beads.....	204
Figure 4.50	TGA and DTG plots of CTAC-CNC/ALG hydrogel beads and CNC	206
Figure 4.51	Surface morphology of pure alginate hydrogel beads and its cross-section (a-b), surface morphology of porous CTAC-CNC/ALG hydrogel beads and its cross-section before adsorption (c-d) and after 4-CP adsorption (e-f).....	208
Figure 4.52	Nitrogen adsorption-desorption isotherm at 77 K obtained for porous CTAC-CNC/ALG hydrogel beads.....	210
Figure 4.53	(a) Point of zero charge (pH_{PZC}) of CTAC-CNC/ALG hydrogel beads in 0.05 M NaCl, and (b) zeta potential (mV) of CNC/ALG and CTAC-CNC/ALG hydrogel beads obtained at pH 7	213
Figure 4.54	(a) 4-CP removal (%) of 2 wt.% of ALG containing hydrogel beads with varying wt.% of CNCs (concentration of 4-CP solution = 100 mg L^{-1} , volume of 4-CP solution = 100 mL dosage of hydrogel beads = 0.5 g). (b) 4-CP removal (%) of 1.5 wt.% CNC containing hydrogel beads with varying wt.% of ALG)	215
Figure 4.55	Influence of (a) contact time and (b) adsorbent dosage on 4-CP adsorption behaviour by Cu-CNC/ALG hydrogel beads.....	217
Figure 4.56	Influence of ionic strength on 4-CP adsorption with regards to Cu-CNC/ALG hydrogel beads.....	219
Figure 4.57	Influence of initial 4-CP concentration on its adsorptive removal efficacy with regards to Cu-CNC/ALG hydrogel beads.....	221
Figure 4.58	Influence of solution pH on the adsorptive removal efficacy of 4-CP with regards to Cu-CNC/ALG hydrogel beads	222
Figure 4.59	(a) Non-linear and (b) linear Langmuir isotherm, (c) non-linear and (d) linear Freundlich isotherm, (e) Temkin and (f) Dubinin-Radushkevich isotherm plots representing the adsorption of 4-CP onto Cu-CNC/ALG hydrogel beads	225
Figure 4.60	(a) Effect of temperature on the adsorption of 4-CP onto Cu-CNC/ALG hydrogel beads (Conditions: pH = 7, adsorbent dose = 0.5 g, initial 4-CP concentration = 100 mg L^{-1} ; contact time = 3 h), and	

	(b) van't Hoff plot of $\ln K_o$ against $1/T$ for 4-CP adsorption onto Cu-CNC/ALG hydrogel beads.....	230
Figure 4.61	Non-linear pseudo-first-order and pseudo-second-order kinetic models fitting for batch adsorption of 4-CP with varying initial 4-CP concentrations by Cu-CNC/ALG hydrogel beads.....	233
Figure 4.62	(a) Plot of q_t vs. time for various 4-CP concentrations and (b) pseudo-second-order (model I) kinetic model fitting for batch adsorption of 4-CP under various initial 4-CP concentrations on Cu-CNC/ALG hydrogel beads.....	235
Figure 4.63	(a) Pseudo-first-order and (b) Elovich plots for batch adsorption of 100 mg L^{-1} 4-CP solution onto Cu-CNC/ALG hydrogel beads	237
Figure 4.64	Plot of $\ln (q_e - q_t)$ versus time (t) with regards to Cu-CNC/ALG hydrogel beads for (a) 50 mg L^{-1} , (b) 200 mg L^{-1} , (c) 400 mg L^{-1} , (d) 600 mg L^{-1} , (e) 800 mg L^{-1} and (e) 1000 mg L^{-1} initial 4-CP concentration at $30 \text{ }^\circ\text{C}$	238
Figure 4.65	Pseudo-second-order (model II) kinetic model fitting for batch adsorption of 4-CP under various initial 4-CP concentrations on Cu-CNC/ALG hydrogel beads.....	239
Figure 4.66	Plot of q_t versus $\ln (t)$ (Elovich isotherm) with regards to Cu-CNC/ALG hydrogel beads for (a) 50 mg L^{-1} , (b) 200 mg L^{-1} , (c) 400 mg L^{-1} , (d) 600 mg L^{-1} , (e) 800 mg L^{-1} and (e) 1000 mg L^{-1} initial 4-CP concentration at $30 \text{ }^\circ\text{C}$	240
Figure 4.67	(a) Weber-Morris plots for batch adsorption of 100 mg L^{-1} 4-CP solution onto Cu-CNC/ALG hydrogel beads and (b) plot of $\log k_{id}$ against \log (initial 4-CP concentration).....	242
Figure 4.68	Plot of q_t versus $t^{0.5}$ (Weber-Morris plot) pertaining to Cu-CNC/ALG hydrogel beads for (a) 50 mg L^{-1} , (b) 200 mg L^{-1} , (c) 400 mg L^{-1} , (d) 600 mg L^{-1} , (e) 800 mg L^{-1} and (e) 1000 mg L^{-1} initial 4-CP concentration at $30 \text{ }^\circ\text{C}$	244
Figure 4.69	EDX analysis for Cu-CNC/ALG hydrogel beads (a) before and (b) after 4-CP adsorption	245
Figure 4.70	Proposed mechanism of adsorption depicting the interaction forces between Cu-CNC/ALG hydrogel beads with 4-CP	247
Figure 4.71	TGA and DTG plots of Cu-CNC/ALG hydrogel beads	248

Figure 4.72	(a) Surface morphology of Cu-CNC/ALG hydrogel beads and (b) its cross-section	249
Figure 4.73	Nitrogen adsorption-desorption isotherm at 77 K obtained for porous Cu-CNC/ALG hydrogel beads.....	250
Figure 4.74	(a) Point of zero charge (pH_{PZC}) of Cu-CNC/ALG hydrogel beads in 0.05 M NaCl and (b) zeta potential (mV) of CNC/ALG and Cu- CNC/ALG hydrogel beads obtained at pH 7	252
Figure 4.75	Regeneration yields of (a) CTAC-CNC/ALG hydrogel beads and (b) Cu-CNC/ALG hydrogel beads corresponding to 4-CP adsorption.....	254

LIST OF ABBREVIATIONS

Symbol	Description
4-CP	4-Chlorophenol
ALG	Alginate
ATR	Attenuated Total Reflectance
BDTDA	Benzyltetradecyl ammonium chloride
BET	Brunauer-Emmett-Teller
BJH	Barrett-Joyner-Halenda
CaP	Calcium phosphate
CNC	Cellulose nanocrystals
CNF	Cellulose nanofibers
CP/MAS	Cross-Polarization/Magic Angle Spinning
CrI	Crystallinity index
CTAC	Cetyltrimethylammonium chloride
D-R	Dubinin-Radushkevich
DSC	Differential Scanning Calorimetry
DTG	Derivative thermogravimetry
EDX	Energy Dispersive X-ray
FTIR	Fourier Transform Infrared

HDTMA	Hexadecyltrimethyl ammonium bromide
IUPAC	International Union of Pure and Applied Chemistry
MCC	Microcrystalline cellulose
NMR	Nuclear Magnetic Resonance
OPB	Oil palm bark
OPEFB	Oil palm empty fruit bunches
OPFFB	Oil palm fresh fruit bunches
OPF	Oil palm frond
OPL	Oil palm leaves
OPMF	Oil palm mesocarp fiber
OPSS	Oil palm sewage sludge
OPT	Oil palm trunk
PFO	Pseudo-first-order
PKS	Palm kernel shell
POME	Palm oil mill effluent
PPF	Palm pressed fiber
ppm	Parts per million
PSO	Pseudo-second-order
PZC	Point of zero charge
RMSE	Root mean square error

rpm	Rotations per minute
RSS	Residual sum of squares
SEM	Scanning Electron Microscope
TEM	Transmission Electron Microscope
TGA	Thermogravimetric Analysis
TTAB	Tetradecyl trimethyl ammonium bromide
UV	Ultraviolet
XPS	X-ray Photoelectron Spectroscopy
XRD	X-ray Diffraction

LIST OF SYMBOLS

%	Percentage	-
K_F	Freundlich adsorption constant	$(\text{mg/g})(\text{L/g})^{1/n}$
ΔG	Gibbs free energy change	kJ mol^{-1}
ΔH	Enthalpy change	kJ mol^{-1}
ΔH_T	Heat of adsorption	J mol^{-1}
ΔS	Entropy change	$\text{J mol}^{-1} \text{K}^{-1}$
a_e	Initial rate of adsorption	$\text{mg g}^{-1} \text{min}^{-1}$
b_e	Adsorption constant (Elovich)	g mg^{-1}
B_T	Temkin isotherm constant (heat of adsorption)	J mol^{-1}
C	Adsorption constant (Weber-Morris)	mg g^{-1}
$^{\circ}\text{C}$	Degree of Celsius	-
C_e	Equilibrium concentration of adsorbate	mg L^{-1}
C_0	Initial concentration of adsorbate	mg L^{-1}
C_t	Concentration at contact time t	mg L^{-1}
E	Mean free energy of adsorption	kJ mol^{-1}
k_1	Pseudo-first-order rate constant	min^{-1}
k_2	Pseudo-second-order rate constant	$\text{g mg}^{-1} \text{min}^{-1}$
k_{2i}	Initial adsorption rate constant	$\text{mg g}^{-1} \text{min}^{-1}$

k_{id}	Intra-particle diffusion rate constant	$\text{mg g}^{-1} \text{min}^{-0.5}$
K_L	Langmuir adsorption constant	L mg^{-1}
K_T	Temkin isotherm constant (binding energy)	L g^{-1}
n	Heterogeneity factor	-
pH_f	Final pH	-
pH_i	Initial pH	-
q_e	Equilibrium adsorption capacity	mg g^{-1}
$q_{e,cal}$	Calculated adsorption capacity	mg g^{-1}
$q_{e,exp}$	Experimental adsorption capacity	mg g^{-1}
q_m	Maximum adsorption capacity	mg g^{-1}
q_t	Adsorption capacity at a given time t	mg g^{-1}
R	Universal gas constant	$\text{J mol}^{-1} \text{K}^{-1}$
R^2	Correlation coefficient	-
R_L	Langmuir isotherm separation factor	-
T	Absolute temperature	K
t	Time	min or h
T_m	Melting temperature	K
V	Volume	L
W	Weight	g

Greek letters

χ^2	Reduced Chi-square	-
ε	Polanyi potential	J mol ⁻¹
β	D-R adsorption constant	mol ² kJ ⁻²
λ	Wavelength	nm

**MANIK HIDROGEL SELULOSA NANOHABLUR-ALGINAT BERFUNGSI
DARIPADA PELEPAH KELAPA SAWIT BAGI PENJERAPAN 4-
KLOROFENOL DALAM LARUTAN AKUEUS**

ABSTRAK

4-klorofenol (4-CP) sebagai bahan kimia pengganggu endokrin fenolik (EDC) merupakan salah satu bahan cemar yang paling biasa dikesan dalam sumber air, yang juga terkenal dengan ketoksikan tinggi dan kekarsinogenan. Klorofenol telah dieksploitasi secara meluas sebagai pengawet dalam industri kayu, gentian, cat, dan industri kulit, digunakan sebagai pembasmi kuman, serta digunakan dalam penghasilan industri pengawet, racun herba, racun perosak dan pewarna, yang seterusnya berakhir di dalam air. Oleh itu, kajian ini bertujuan untuk membangunkan manik hidrogel berasaskan nanohablur selulosa yang cekap dalam merawat air sisa simulasi yang tercemar dengan 4-klorofenol. Pada mulanya, nanohablur selulosa (CNC) telah diekstrak daripada pelepah kelapa sawit (OPF) menggunakan kaedah hidrolisis asid sulfurik bersama-sama dengan pelbagai prarawatan. CNC yang diekstrak telah dicirikan melibatkan pelbagai teknik pelengkap, seperti FTIR, keadaan pepejal ^{13}C NMR, TGA, DSC, XRD, SEM-EDX, TEM dan analisis BET bagi mengesahkan ketulenannya. CNC kemudiannya dirumuskan dalam bentuk manik hidrogel menggunakan matriks biopolimer alginat. Di samping itu, dua bentuk manik hidrogel alginat berasaskan CNC yang diubah suai telah dihasilkan, iaitu setiltrimetilamonium klorida (CTAC)-terubah suai CNC dan CNC terubah suai kuprum. Bahan ini telah dicantumkan pada asas alginat (ALG) bagi meningkatkan kecekapan, julat pH terpakai dan kapasiti penjerapan. Manik hidrogel CNC/ALG bentuk yang tidak diubah suai dan diubah suai telah dicirikan oleh pelbagai teknik pelengkap, termasuk FTIR, SEM, XPS, TGA, ukuran luas permukaan/keliangan,

potensi zeta dan analisis pH_{pzc} . Keputusan pencirian menunjukkan rangkaian liang yang dipertingkatkan dan kestabilan strukturnya. Penyingkiran penjerap 4-CP telah dioptimumkan dengan mengubah pelbagai keadaan eksperimen, seperti masa silangan, saiz manik, dos penjerap, kepekatan awal 4-CP, pH sederhana, kelajuan pengacauan, masa sentuhan, suhu, keupayaan penjanaaan semula dan kebolegunaan semula. Keputusan yang diperoleh menunjukkan bahawa persamaan dengan kadar tertib pseudo-kedua dan isoterma penjerapan Langmuir telah digambarkan penjerapan 4-CP pada manik hidrogel ALG berasaskan CNC. Kapasiti penjerapan maksimum yang dicapai bagi sampel tidak diubah suai, CTAC-CNC diubah suai dan tembaga-CNC diubah suai masing-masing ialah 19.168, 64.935 dan 66.667 mg g⁻¹. Kajian kebolegunaan semula mendedahkan bahawa manik hidrogel berasaskan CNC yang diubah suai boleh digunakan semula sehingga lima kitaran berulang. Kajian termodinamik menunjukkan bahawa proses penjerapan adalah eksotermik, spontan dan boleh diterbalikkan dalam julat suhu yang dianalisis 303 hingga 323 K. Model Weber-Morris mendedahkan bahawa resapan intrapartikel bukanlah langkah pengawalan kadar tunggal dalam proses penjerapan. Mekanisme penjerapan yang membawa kepada proses penjerapan yang berkesan ialah penjerapan pengisi liang, ikatan hidrogen, interaksi elektrostatik, anion- π dan π - π tindanan. Keputusan menunjukkan bahawa manik hidrogel CNC/ALG berfungsi boleh digunakan sebagai penjerap yang mampan dan berkesan bagi pemulihan 4-CP.

**FUNCTIONAL CELLULOSE NANOCRYSTAL-ALGINATE HYDROGEL
BEADS PREPARED FROM OIL PALM FRONDS FOR THE ADSORPTION
OF 4-CHLOROPHENOL IN AQUEOUS SOLUTION**

ABSTRACT

4-chlorophenol (4-CP), being a phenolic endocrine-disrupting chemical (EDC), which is well known for its high toxicity and carcinogenicity, is one of the most commonly detected pollutants in water resources. Chlorophenols have been extensively exploited as preservatives in wood, fibers, paints, and leather industries, used as disinfectants, as well as utilized in the industrial production of preservatives, herbicides, pesticides, and dyes, which consequently end up in water bodies. Hence, the present study aimed to develop efficient cellulose nanocrystal-based hydrogel beads in treating simulated wastewater contaminated with 4-chlorophenol. Initially, cellulose nanocrystals (CNCs) were extracted from oil palm fronds (OPF) employing the sulphuric acid hydrolysis method along with various pretreatments. Extracted CNCs were characterized by using numerous complementary techniques, such as FTIR, solid-state ^{13}C NMR, TGA, DSC, XRD, SEM-EDX, TEM and BET analyses which affirmed the purity. CNCs were then formulated in the form of hydrogel beads using alginate biopolymer matrix. In addition, two modified forms of CNC-based alginate hydrogel beads were prepared, which are cetyltrimethylammonium chloride (CTAC)-modified CNC and copper-modified CNC. They were grafted onto the backbone of alginate (ALG) in order to enhance the efficiency, applicable pH range and adsorption capacity. The unmodified and modified forms of CNC/ALG hydrogel beads were characterized by various complementary techniques, including FTIR, SEM, XPS, TGA, surface area/porosity measurement, zeta potential and pH_{pzc}

analyses. Characterization results revealed the enhanced pore network and its structural stability. The adsorptive removal of 4-CP was optimized by altering various experimental conditions, which are crosslinking time, bead size, adsorbent dosage, initial 4-CP concentration, medium pH, stirring speed, contact time, temperature, regeneration capability and reusability. Obtained results revealed that the pseudo-second-order rate equation and the Langmuir adsorption isotherm best described the adsorption of 4-CP onto CNC-based ALG hydrogel beads. The maximum adsorption capacities achieved for unmodified, CTAC-CNC modified, and copper-CNC modified were 19.168, 64.935 and 66.667 mg g⁻¹, respectively. The reusability study revealed that modified forms of CNC-based hydrogel beads could be reused up to five repeated cycles. The thermodynamic study indicated that the adsorption process was exothermic, spontaneous, and reversible within the analyzed temperature range of 303 to 323 K. The Weber-Morris model revealed that intraparticle diffusion was not the sole rate-controlling step in the adsorption process. The adsorption mechanisms leading to an effective adsorption process were adsorptive pore-filling, hydrogen-bonding, electrostatic interaction, anion- π and π - π stacking. The results revealed that functional CNC/ALG hydrogel beads could be employed as sustainable and effective adsorbents for 4-CP remediation.

CHAPTER 1

INTRODUCTION

1.1 Research background

Owing to the ever-growing human population, unskilled usage of natural water resources (De Gisi et al., 2016), climate change (Diyaniilla et al., 2020), and rapid urbanization, which is indispensable for all aspects of human life, the quality of water has deteriorated significantly over the past few decades causing water a scarce source (Putro et al., 2017). According to United Nations Sustainable Development Goals 2019 report, over 2 billion people live in countries experiencing high water stress, and by 2030, 700 million people could be displaced by intense water scarcity (Ismail & Go, 2021). Moreover, since the past few decades have witnessed staggering growth in industrialization, agricultural and domestic activities globally, it has posed a severe menace to the environment and human health, especially the detrimental effects provoked on flora and fauna. The main cause of these detrimental effects is due to the direct discharge of a wide array of hazardous contaminants or pollutants, for instance, toxic inorganic anions, synthetic dyes, pesticides, micropollutants and organics into natural waterbodies (Beyki et al., 2016).

Chlorophenols are used broadly as dyes, preservatives, fungicides, herbicides, algicides, insecticides, and pharmaceuticals. Usually, most chlorophenolic compounds are persistent toxic substances, which threaten human health through direct contact and bio-accumulation. Contamination by chlorophenols in air, soils, natural waters, and other waterbodies has caused widespread concern. It has been reported that long-term consumption of chlorophenol-adulterated water stimulates particularly anemia

and dizziness among other symptoms, and can even affect the central nervous system and liver (Lei et al., 2021). Despite most of the chlorophenols being bio-refractory pollutants, they have been extensively exploited as preservatives in wood, fibers, paints, and leather industries, used as disinfectants, as well as utilized in the industrial production of herbicides, pesticides, phenolic resins and dyes, which consequently end up in groundwater (Wen et al., 2013). Thus, the advancement of competent techniques to remove chlorophenols in water treatment is essential (Peng et al., 2017).

Wastewater treatment refers to a process of separating or removing contaminants from effluent by employing chemical or physical methods ahead of discharging them into the environment (Jain et al., 2021). Introducing strongly sorptive and/or reactive solids into aquifers is a widely used engineering scheme for in situ remedies of groundwater systems contaminated with toxic organic and inorganic chemicals. These solids not only are highly reactive but also can remain suspended and can travel along with groundwater in polluted aquifers over extended periods of operating time. Therefore, searching for innovative nanomaterials that meet the two criteria has long remained a top priority in the field of groundwater remediation (Chen et al., 2017). Adsorption-based water purification technology is attractive because it is amenable to various contaminant concentrations and contaminant feeding conditions without affecting the contaminant removal efficiency. Given that the cost of adsorption technology is mainly associated with the adsorbent, a proper adsorbent should be selected to realize an economically viable treatment process. Therefore, the development of low-cost adsorbents that can yield high removal efficiency is important (Kumar et al., 2018). However, most natural wastes do not offer high adsorption performance due to relatively low specific surface area and undesirable uptake capacity. During the last decade, nanomaterials have emerged as potential

adsorbents for environmental remediation and wastewater treatment and have aroused increasing attention to face environmental issues (Mahfoudhi & Boufi, 2016).

Moreover, the current practice of passive dumping and open burning of unwanted matured oil palm fronds in large plantations is aesthetically displeasing (Onoja et al., 2019) and contributes to degraded regional air quality along with increased health problems (Jain et al., 2014). Such methods for disposing of enormous quantities of agricultural biomass are environmentally challenging as well as unsustainable in the long run. Moreover, the full benefits of oil palm biomass are not fully explored, representing a valuable source of renewable cellulosic materials, viz., cellulose, hemicelluloses, and lignin (Elias et al., 2018). Nanocellulose refers to materials with a diameter of 5-20 nm obtained from cellulose (Manna et al., 2018). Nanocelluloses are used in various applications due to their low density, low cost, abundance, renewability, high mechanical properties, large surface area and aspect ratio, considerable flexibility, specific barrier properties and low thermal expansion (Abdul Khalil et al., 2016). In addition, it has been proved that nanocellulose can be classified as a non-toxic material (Vartiainen et al., 2011), 100% biodegradable and has no side effects on the environment (Bhatnagar et al., 2015). It is well known that nanocellulose-based beads provide considerable benefits over commercial adsorbents for water pollution control, including ease of separation, availability of abundant functional groups, biodegradability and eco-friendly (Abou-Zeid et al., 2021; Mohammed et al., 2015; Zhao et al., 2021).

1.2 Problem statements

Most of the phenolic compounds present in the waste streams of a wide variety of industrial operations are toxic, and some are carcinogens. They get into the food chain and pose serious environmental threats. Chlorinated phenols (CPs) are widely used in chemical, petrochemical, plastic, leather, paint, pharmaceutical, and steel industries. The increasing use of these compounds leads to environmental pollution because of their high solubility and low biodegradability. Chlorophenols with two or more chlorines are often used as pesticides or derivatized to convert them into pesticides. Sometimes they are also used as antiseptic agents. Moreover, chlorophenols, especially 4-chlorophenol, have been used as antiseptics. They are also used as wood preservatives (Manna, 2018; Yousef & El-Eswed, 2009). Thus, there are several diverse ways in which people can get exposed to chlorophenols. On the whole, 4-chlorophenol was desired as the target contaminant for specific reasons that it is highly poisonous to aquatic life, humans, and plants even at low concentration levels, persistent in the environment due to stability of its structure, widespread use in numerous industries (including in producing textile dyes, polymeric resins, wood preservatives, fungicides, biocides, pesticides) and is typically found in drinking water (Garba & Rahim, 2016). Besides, based on the past literature, a minimal number of studies have been carried out on the removal of 4-chlorophenol in particular as opposed to other environmental pollutants, including heavy metal ions and dyes.

The most widely used method to treat phenols contaminated wastewater is adsorption onto the surface of activated carbon. However, the high cost associated with activated carbon in terms of initial and regeneration costs makes it undesirable to be employed on a large scale (Chen et al., 2017). Thus, there is a need for more

economical and environmentally friendly methods for improved adsorption rate of chlorophenols. Moreover, most of the industrial adsorbents engaged currently are in the form of porous macro-sized particles to increase the surface area and enhance the adsorption capacity (Mahfoudhi & Boufi, 2017). However, diffusion within the particles has limitations and can lead to a decrease in the adsorption capacity and rate. Moreover, adsorbents must be easily separated from the effluent and should be easily regenerated with a minimum loss in the adsorption capacity. This issue is even more amplified for nanosized adsorbents. Hence, the preparation methods and the influence of experimental conditions need to be optimized to achieve high adsorption capacity.

Malaysia, an agricultural country, which serves as the world's second-largest palm oil producer and exporter after Indonesia, confronts the challenges of disposing of waste generated from palm oil production. The oil palm biomass by-products are overage and abandoned as wastes, which are stacked to rot, impacting environmental pollution. Despite the high energy-producing ability of oil palm fronds (OPF), it is the least utilized out of all the biomass produced. Thus, valorization of these wastes and converting them into viable products and sustaining cost are essential and economically beneficial to the nation, which could promote Malaysia's contribution to settling the global pollution crisis. Moreover, in view of the major drawbacks in current methods for disposing of OPF biomass, the development of new technological applications has widened the utilization of OPF, which has caught much attention among the scientific community. In addition, it also conforms with the "Zero Waste" initiative illustrated by the Malaysian Palm Oil Board (Ng et al., 2012). The "Zero Waste" initiative can be practiced to convert the widely available undesirable biomass into functional materials with potential industrial applications (Elias et al., 2018).

1.3 Research objectives

In order to address the shortcomings mentioned above, this study aims to propose a facile method for the preparation of environmentally friendly and efficient cellulose nanocrystals-based hydrogel beads with minimum chemical usage, short reaction time and low temperature. The following research objectives were targeted to be accomplished in this research study:

- 1) To isolate cellulose nanocrystals from oil palm fronds and characterize using various techniques.
- 2) To functionalize cellulose nanocrystals and prepare them in the form of hydrogel beads, characterize hydrogel bead adsorbents and enhance their porosity.
- 3) To optimize the adsorption parameters of the unmodified/modified hydrogel beads towards 4-chlorophenol.
- 4) To characterize experimental data with adsorption isotherm models, investigate the kinetics of adsorption based on 4-chlorophenol's uptake performance, probe various thermodynamic parameters at different temperatures, such as enthalpy (ΔH^0), Gibbs free energy (ΔG^0) and entropy (ΔS^0) changes through thermodynamic study, to elucidate mechanisms involved in the adsorption of 4-chlorophenol, and to infer the reusability of modified cellulose nanocrystal-alginate hydrogel beads through adsorption-desorption cycles.

1.4 Scope of study

This study consists of investigating the potentials of cellulose nanocrystals (CNCs) and two of their functionalized forms (quaternary ammonium salt modification and copper modification) as fillers for the preparation of hydrogel beads

from oil palm fronds using sodium alginate (ALG) as the biopolymer matrix. Cellulose nanocrystals will be extracted from oil palm fronds using a three-step process, which involves alkali treatment, bleaching and acid hydrolysis. Isolated cellulose nanocrystals will be characterized using various complementary techniques to affirm their purity. An ionotropic gelation method involving a Ca^{2+} crosslinker will be used to fabricate CNC-based hydrogel beads. Modified and unmodified hydrogel beads will be optimized with the aid of preparation conditions, especially CNC: ALG ratio and various experimental conditions. The efficacy of the optimal hydrogel beads will also be investigated by the adsorption of 4-chlorophenol. The optimized hydrogel beads will be characterized to ascertain the functional groups present, specific surface area, thermal stability, elemental composition, binding energy, and surface morphology.

The study covers single batch adsorption experiments, which will focus on investigating the effects of agitation speed (50-500 rpm), hydrogel bead size (2.1, 2.9 and 3.8 mm), crosslinking time (15-120 min), solution pH (2-12), temperature (30-50 °C), initial 4-chlorophenol solution concentration (50-1000 mg L⁻¹) and adsorbent dosage (0.25-5.0 g). Langmuir (type I-IV), Freundlich, Temkin and Dubinin-Radushkevich adsorption isotherm mathematical models, as well as kinetic models (pseudo-first-order, pseudo-second-order, Elovich and intraparticle diffusion), will be employed to investigate the equilibrium and kinetics data. Thermodynamic parameters (Gibbs free energy, enthalpy, and entropy) will also be determined, and their influence on the adsorption processes will be assessed. Regeneration of the spent hydrogel beads will be experimented with repeated adsorption cycles.

1.5 Gap of knowledge

The application of cellulose nanocrystal/alginate hydrogel beads in the field of adsorption for the removal of 4-chlorophenol is yet to be explored to the best of our knowledge. In addition, most industrial adsorbents employed currently are in the form of porous macro-sized particles, which limit their application for the detoxification of contaminants present in low concentration. Hence, the primary goal of the present research study is to prepare functional mesoporous cellulose nanocrystal/alginate hydrogel beads with high porosity for the adsorptive removal of 4-chlorophenol in aqueous media.

1.6 Thesis outline

The thesis is structured into five chapters and a section for references and appendices. The summarized thesis organization is as follows:

Chapter 1 includes the background of the study, problem statement, research objectives and scope of the study. Chapter 2 reviews literature pertaining to the challenges faced with water pollution and various methods used in tackling wastewater with emphasis on adsorption from its fundamental principles. Advancements and challenges in the use of adsorption for wastewater treatment are discussed. Batch adsorption systems with their various forms of analysis such as isotherms, kinetics, mechanism, and thermodynamics are also highlighted in this chapter. Chapter 3 comprises all the materials and equipment used in the present study and a detailed description of the experimental setup and experimental procedure. This includes the extraction of cellulose nanocrystals and characterization, preparation of unmodified

and functional cellulose nanocrystal/alginate hydrogel beads, characterization of hydrogel beads, and design of experiments as well as batch adsorption and regeneration studies.

Chapter 4 presents the collated results of chapter 3 experimental work and elaborated discussion. The chapter is divided into four sections which are (i) experimental design and optimization results, (ii) characterization results, (iii) batch adsorption studies, and (iv) desorption and regeneration studies. Detailed analysis of adsorption isotherms, kinetic models, mechanism, and adsorption thermodynamics are also presented. The capability of using cellulose nanocrystal/alginate-based hydrogel beads is also presented and discussed. Chapter 5 concludes the findings from the present study concerning the objectives of this study and recommendations drawn from the research work.

CHAPTER 2

LITERATURE REVIEW

2.1 Oil palm biomass

Oil palm (*Elaeis guineensis* Jacquin) tree, an agricultural plant, has succeeded in becoming one of the commodity oil crops that insure Malaysia's economic development (Lamaming et al., 2015). In 2015, the annual production of crude palm oil in Malaysia stood at 20.5 million metric tons (Lee et al., 2020) in terms of global palm oil supply, in which 90% corresponded to the generation of a range of oil palm biomass wastes (Ahmad et al., 2016; Lee et al., 2020; Loh, 2017), including oil palm fronds (OPF), oil palm empty fruit bunch (OPEFB), oil palm leaves (OPL), oil palm mesocarp fiber (OPMF), also known as palm pressed fiber (PPF), oil palm bark (OPB), palm kernel shell (PKS), palm oil mill effluent (POME), also known as oil palm sewage sludge (OPSS), oil palm fresh fruit bunches (OPFFB), and oil palm trunk (OPT) (Brito et al., 2018; Chan et al., 2018; Dungani et al., 2017; Lee et al., 2018; Loh, 2017; Onoja et al., 2019). Figure 2.1 depicts the most generated co-products of oil palm biomass. Dungani et al. (2017) noted that OPF contributes to 70% (wt.) of total oil palm biomass waste. Tahir et al. (2018) reported that annual oil palm production in Malaysia is expected to increase up to 50 million tons by 2030. Since the oil palm industry is the largest contributor of biomass in Malaysia (Abnisa et al., 2013), annually, large amounts of oil palm biomass wastes are air burnt or discarded at the plantations without proper utilization upon pruning during oil palm trees replantation and milling processes (Onoja et al., 2019). It is alarming to report that the imprudent disposal of oil palm biomass wastes causes severe environmental impact,

for instance, the unceasing aggregation of OPF at plantation sites potentially threatens the ecosystem owing to the formation of greenhouse gases amid microbial degradation (Dungani et al., 2017).

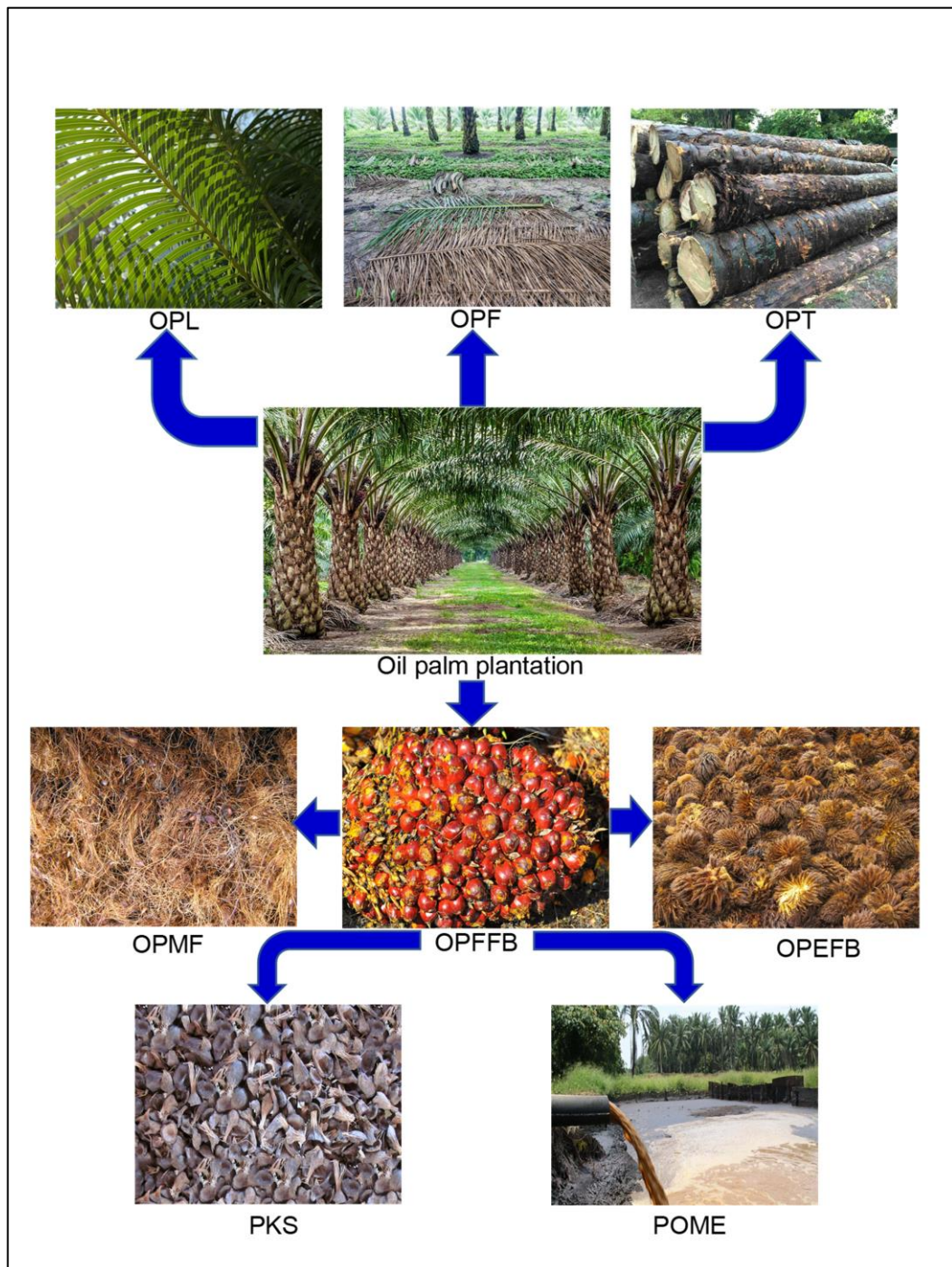


Figure 2.1: Major oil palm biomass residues (adapted from Diyanilla et al. (2020))

Therefore, researchers have come up with the idea of converting the underutilized oil palm bio-fiber into profitable value-added products (Onoja et al., 2019). As oil palm biomass are lignocellulosic materials, they mainly comprise lignin and cellulose. The potential exploitation of oil palm fibers as a source to extract cellulose would uplift the economy of farmers and stamp out the imprudent disposal of oil palm biomass wastes. These cellulose fibers can be utilized to produce cellulose nanocrystals (CNCs) (Dungani et al., 2017). Hamzah et al. (2019) reported that the total oil palm biomass residues (dry weight basis) available for pruning, replanting, and milling activities in Malaysia in 2017 (Figure 2.2) accounted for 51.19 metric tons (Mt) based on 101.02 Mt of oil palm fresh fruit bunches (OPFFB) processed. According to Figure 2.2, OPF is the most significant oil palm biomass residue.

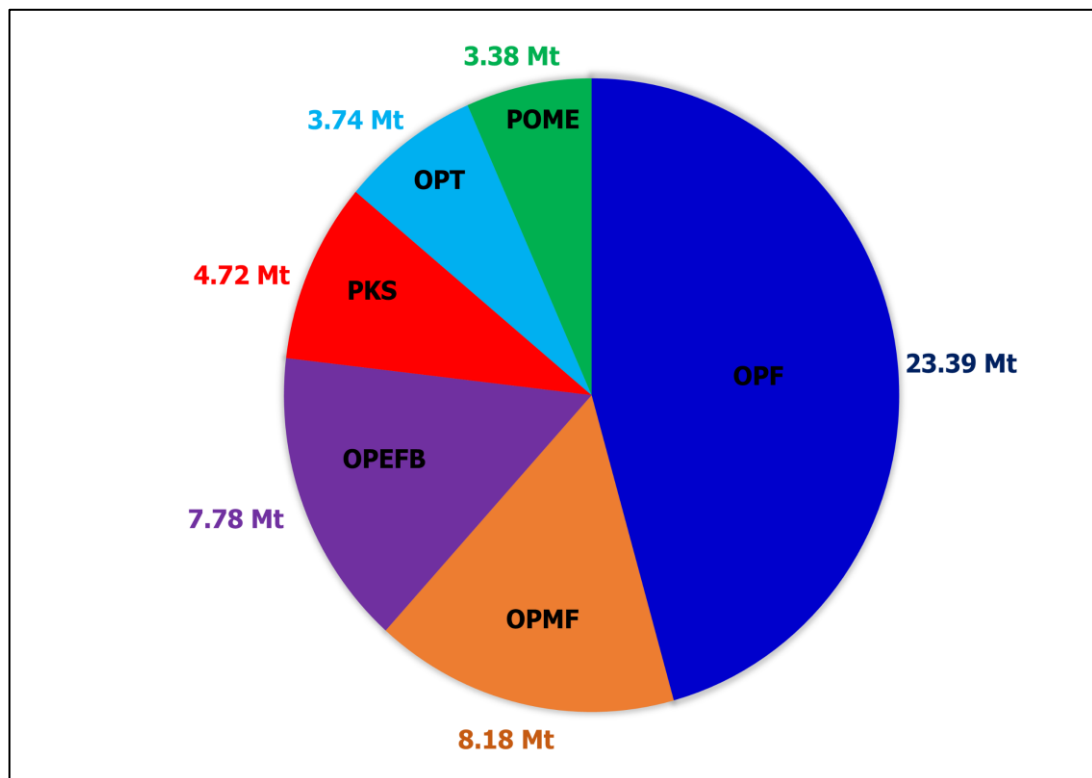


Figure 2.2: Availability of major oil palm biomass residues in Malaysia in 2017 (adapted from Diyanilla et al. (2020))

Table 2.1 outlines the lignocellulosic composition and extractives content based on different components of the oil palm tree.

Table 2.1: Lignocellulosic composition and extractives content of oil palm fronds based on previous research studies

Extractives (%)	Lignin (%)	Cellulose (%)	Hemicellulose (%)	References
4.27	20.00	40.03	27.08	Azani et al. (2020)
-	17.72	54.66	23.52	Saurabh et al. (2016)
3.50	20.15	47.76	35.37	Hashim et al. (2011)
-	15.20	32.70	22.50	Zakaria et al. (2015)
20.60	19.70	42.80	-	Tan et al. (2016)
-	25.00	31.00	24.00	Wan Omar and Amin (2016)
11.33	19.53	44.80	-	New et al. (2019)
-	21.70	50.33	23.18	Abnisa et al. (2013)
-	26.00	26.40	47.60	Mahmood et al. (2016)
-	24.62	35.73	28.39	Hussin et al. (2016)
-	23.30	39.50	23.60	Lawal et al. (2021)
-	18.42	41.25	23.95	Ong et al. (2021)
-	18.07	39.84	21.83	Lee et al. (2021)
-	17.80	41.40	20.10	Tnah et al. (2022)

OPF residue is currently used in various industries such as the production of brooms. The low energy density of oil palm residues (especially OPF and PKS) has made possible today's advancement in the briquetting process to produce better fuel for future power generation (Kaniapan et al., 2021). OPF is also used as mulches for

soil erosion control and nutrients conservation (Tang & Qahtani, 2020). Ironically, discovery in alternative uses or values of oil palm biomass wastes is often translated as evidence for sustainability of oil palms though still at research and development stage. In the recent past, many attempts have been undertaken to unravel the potential utilization of OPF, including butanol production as a fuel alternative (Mahmud & Rosentrater, 2022), bio-oil and biochar production (Chantanumat et al., 2022), clean syngas (H_2+CO) production (Inayat et al., 2021), as a reinforcing filler (CNC-OPF) for mild steel corrosion protection (Azani et al., 2020), for solid biofuels (Kongto et al., 2022), nonsevere furfural production (Lee et al., 2021), activated carbon production (Maulina et al., 2020), and for the development of fertilizers (Phoochinda, 2020). These are some evidence of technological progress in the valorization of oil palm frond biomass as the main feedstock for value-added bioproducts. Hence, it is evident that OPF biomass generated has attracted great interest from researchers due to the abundance of this valuable material which can be converted into value-added materials such as bioelectricity, biofuels, biohydrogen, bioplastics, biosugars, and nanocellulose (Norrrahim et al., 2022).

2.2 Overview of nanocellulose

Cellulose is the most ubiquitous naturally occurring biopolymer on the planet earth, produced mainly by plants, algae, fungi, bacteria, and tunicates (Buffiere et al., 2017; George & Sabapathi, 2015; Rodríguez et al., 2011), is renewable, biologically degradable, non-toxic (Dufresne, 2013) as well as water-insoluble (Trache et al., 2020). The word “cellulose” has been derived from a French word, “cellule”, which refers to a living cell and glucose (Olivera et al., 2016). The promising features of

cellulose make it to be employed as an alternative to non-degradable fossil-fuel-based polymers (George & Sabapathi, 2015). It is a high molecular weight linear homopolymer of 1,4- β -glucose unit linked by glycosidic oxygen bridges (Figure 2.3a), comprised of microfibrils of nano-size diameter and surrounded by lignin and hemicellulose (Mahfoudhi & Boufi, 2016). In view of nourishing the demand for utilizing biocompatible and green materials, cellulose holds a vital position due to being inexhaustible, highly functional and sustainable, and amenable feedstock (Trache et al., 2017). Moreover, cellulose inherits a unique hierarchical structure (Figure 2.3b) to have gained increasing attention to exploring its exclusive properties.

Nonetheless, reasonably poor adsorption capability and limited solubility in water and organic solvents have restricted the technological applications of cellulose (Sehaqui et al., 2016). To improve the adsorption characteristics of cellulose, its specific surface area and the amount of active sites should be increased through the preparation of nanocelluloses (Hong et al., 2019). More importantly, nanocellulosic materials have attracted growing interest due to their well-defined structure and functionalities (Grishkewich et al., 2017). Since the production of nanomaterials derived from petroleum-based resources involves the extensive use of hazardous chemicals and causes global warming and related environmental concerns. Thus, desperate measures have been taken to utilize materials derived from renewable resources instead of conventional raw materials to attain sustainable development (Putro et al., 2017).

Nanocellulose obtained from lignocellulosic materials is endowed with astounding thermal and mechanical properties, as well as they are eco-friendly and cheap to produce (Rambabu et al., 2016). Nanocelluloses are typically nanoscale cellulosic materials with at least one of their dimensions (diameter, length or width)

below 100 nm (Thomas et al., 2020). In recent years, biosorbents, for instance, adsorbents prepared from nanocellulose, have gained increasing attention, being environmentally benign and inexpensive to produce (Beyki et al., 2016). Extensive research work is being executed to convert abundant, cost-effective, and renewable materials to obtain value-added products with significant benefits.

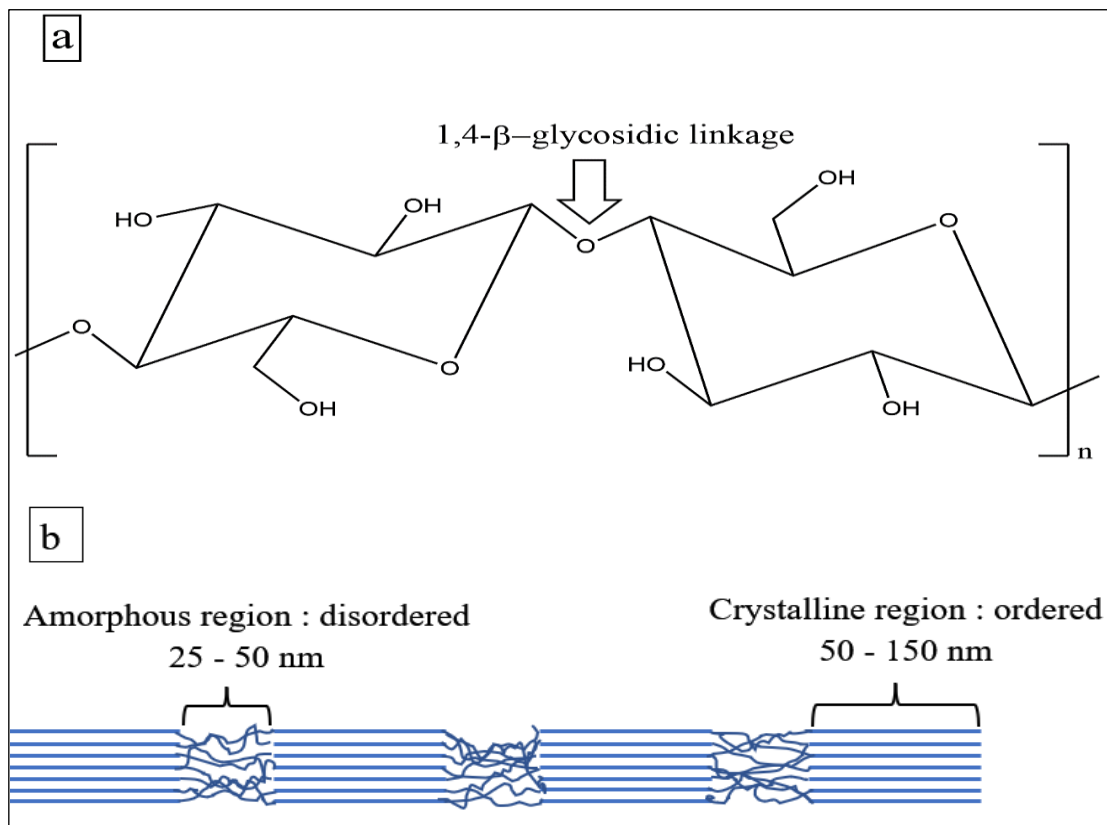


Figure 2.3: a) Chemical structure and b) microstructure of cellulose (Trache et al., 2020)

Nanocelluloses can be classified into three major classes based on their preparation techniques, processing conditions, shape (morphology) and size, which are (i) cellulose nanocrystals (CNC), also known as cellulose nanowhiskers, (ii) cellulose nanofibrils (CNF), also called nanofibrillar cellulose, and (iii) bacterial nanocellulose (BNC), sometimes referred as bacterial cellulose (Mondal, 2017; Yi et al., 2020; Zinge

& Kandasubramanian, 2020). Nanocellulose can be isolated from diverse lignocellulosic plant resources through chemical, mechanical treatments or bacterial origin as individual processes or can be combined to attain nanocelluloses with peculiar characteristics (Espíndola et al., 2021; Mondal, 2017; Phanthong et al., 2018; Trache et al., 2020). Table 2.2 depicts some of the major isolation methods of nanocellulose from cellulose pulp.

Table 2.2: Primary isolation methods/treatments of cellulose pulp-derived nanocellulose

Classification	Pretreatment method	Reference
Chemical	<ul style="list-style-type: none"> • Acid hydrolysis • 2,2,6,6-tetramethylpiperidine-1-oxyl (TEMPO)-mediated oxidation • Alkaline treatment • Ionic liquid treatment • Solvent extraction 	Phanthong et al. (2018)
Physical (mechanical)	<ul style="list-style-type: none"> • Grinding • High-pressure homogenization (microfluidization) • Ultrasonication • Milling (PFI, disk, planetary ball) • Steam explosion • Electrospinning • Micro-jet method 	Wang (2019)
Biological	<ul style="list-style-type: none"> • Enzymatic hydrolysis • Bacteria • Fungi 	Mondal (2017)

There are two key steps involved in the preparation of nanocelluloses. First, the initial pretreatment step involves the delignification of the biomass to reduce its recalcitrance and removal of hemicellulose, which is applied to the lignocellulosic

material to acquire pristine cellulose (Diyanilla et al., 2020) and secondly, treating pristine cellulose by chemical or physical methods, which deconstruct the cellulosic hierarchical structure (Curvello et al., 2019) to yield nanocellulose.

2.3 Cellulose nanocrystals

CNCs are typically produced through mineral acid hydrolysis, viz. concentrated acid breakdown, with the use of H_2SO_4 , H_3PO_4 , HCl , HBr , citric acid and formic acid under regulated conditions of temperature, time and acid to cellulosic fiber ratio (Tshikovhi et al., 2020) with subsequent post-treatment approaches, including centrifugation, neutralization and dialysis to eliminate the excess acid on its surface (Trache et al., 2020; Zinge & Kandasubramanian, 2020). Cellulose nanocrystals can also be produced through recyclable organic acids (especially dicarboxylic acids), including oxalic, maleic, and *p*-toluenesulfonic acids. Enzymatic phosphorylation (Liu et al., 2015) and oxidation (Klemm et al., 2018) are two additional methods employed to prepare cellulose nanocrystals. Despite the fact that acid hydrolysis using sulfuric acid is the oldest process, it remains the most common preparation method for CNCs. A typical approach starts with alkali and bleaching pretreatments, followed by acid hydrolysis. Figure 2.4 depicts a schematic diagram of a pretreatment process applied to lignocellulosic biomass. It was reported that Calvert was the first author who performed the hydrolysis of cellulose in 1855 (Mao et al., 2017). A few decades later, in 1951, Rånby successfully prepared stable colloidal suspensions of cellulose using H_2SO_4 (Nascimento et al., 2018).

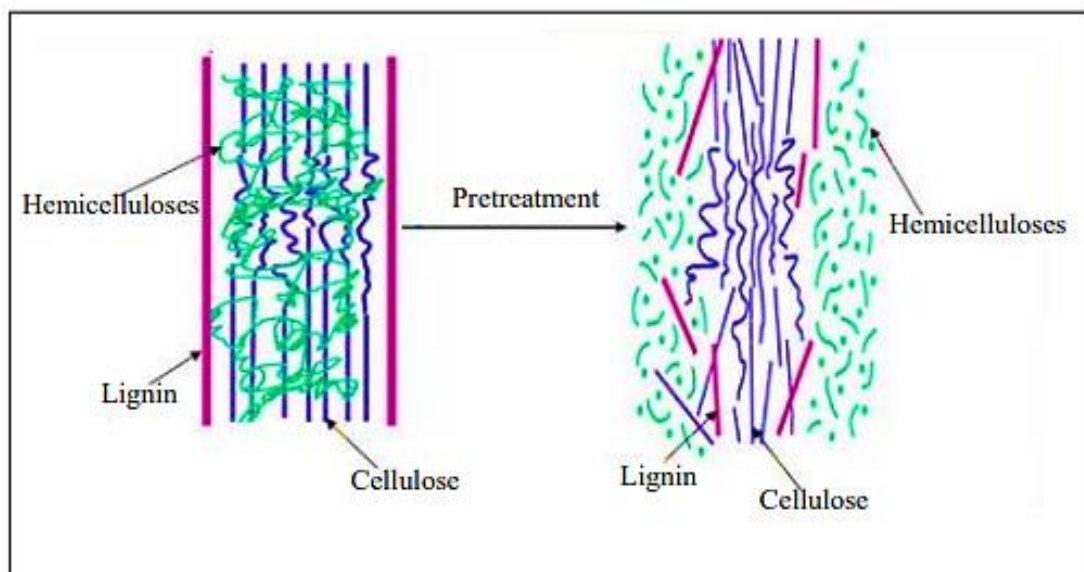


Figure 2.4: Schematic representation of a pretreatment process applied on lignocellulosic biomass (adapted from Sarip et al. (2016))

Since the preparation method and the conditions adopted significantly affect the characteristics of isolated nanocelluloses, Table 2.3 has been presented to highlight the features of diverse nanocelluloses reported in the literature. Depending on the natural source, isolation procedure, conditions, and pre-post-treatments, the characteristics of nanocellulose such as crystallinity, yield, dimensions and morphology, surface chemistry, physicochemical and thermal properties can be tailored for a specific use, opening an extensive range of possibilities to develop new materials (Wohlhauser et al., 2018).

Table 2.3: Effect of isolation method and adopted conditions on the characteristics of CNCs based on recent studies

Source	Isolation treatment	Structural morphology	Dimension (nm)	Zeta potential (mV)	Crystallinity (%)	Degradation temperature (°C)	References
Wheat bran	H ₂ SO ₄ hydrolysis (64 wt.%, 45 °C, 60 min)	Needle-shaped structure	Diameter: 31.2 ± 7.8 Length: 854.7 ± 210.4	NA	NA	NA	Kang et al. (2021)
Commercial MCC	2,2,6,6-tetramethylpiperidine-1-oxyl (TEMPO)-mediated oxidation (pH 10.8, 25 °C, 2 h)	Rod-like structure	Diameter: 8.1 ± 2.0 Length: 96.4 ± 28.8	-35.8 ± 0.6	~58	320-330	R. Sun et al. (2021)
Hardwood kraft pulp	H ₂ SO ₄ hydrolysis (64 wt.%, 45 °C, 2 h)	Needle-like morphology	Hydrodynamic diameter: 172 ± 18	-40.7 ± 0.7	~80	NA	Wang et al. (2021)
<i>Dunaliella tertiolecta</i> marine green algae residue	H ₂ SO ₄ hydrolysis (50 wt.%, 4.5 h)	Needle-like morphology	Diameter: 30 ± 5.2 Length: 520-700	NA	89	369	Mondal et al. (2021)
Almond (<i>Prunus dulcis</i>) shell	TEMPO-mediated oxidation (pH 10, 7 °C, 2 h)	Spherical-like aggregates	Diameter: 25-100	NA	NA	271.4	Maaloul et al. (2021)

Rice husk	H ₂ SO ₄ hydrolysis (10.0 M, 50 °C, 40 min)	Rod-like morphology	Diameter: 5-15 Length: ~400	NA	NA	NA	Supramaniam et al. (2018)
	H ₂ SO ₄ hydrolysis (50 wt.%, 50 °C, 1 h)		NA	-35.73	92.13	345	
Pineapple crown fibers	H ₂ SO ₄ hydrolysis (64 wt.%, 50 °C, 1 h)	Rod-shaped agglomerates	NA	-48.76	84.47	346	Pereira et al. (2020)
	H ₂ SO ₄ hydrolysis (64 wt.%, 50 °C, 2 h)		NA	-47.96	87.44	348	
Cotton linters	H ₂ SO ₄ hydrolysis (65 wt.%, 63 °C, 30 min)	Rod-like nanoparticles	Diameter: 27± 12.4 Length: 129 ± 60.6	-34 ± 5	NA	NA	Lin et al. (2021)
Eucalyptus pulpboard	Enzymatic hydrolysis (10 U mL ⁻¹ xylanase and cellulase enzyme composite, 12 h, 50 °C and 150 rpm)	Rod-shaped	Diameter: 20 Length: 400-500	-25.2	76.6	NA	J.T. Xu et al. (2021)
	Enzymatic hydrolysis (300 U mL ⁻¹ xylanase and cellulase enzyme composite, 4 h, 50 °C and 150 rpm)	Spherical	Diameter: 30	-28.2	55.8	NA	

Grape pomace	Deep eutectic solvent (lactic acid: choline chloride; 2:1 molar ratio) hydrolysis (80 °C, 300 rpm, 6 h)	Rod-like crystals	Diameter: 22.0 ± 3.9 Length: 241.5 ± 45.3	-29.07 ± 1.66	95.2	>380	Fan et al. (2020)
Commercial MCC	Mechanical milling (6 h) with 1000 rpm centrifugal separation	Stacked rod-shaped	Diameter: 43 ± 12 Length: 537 ± 197	-8	NA	NA	Yao et al. (2020)

Note: NA, information is not available

Chen et al. (2016) demonstrated that CNCs produced from bleached eucalyptus kraft pulp employing oxalic acid (70 wt.%, 100 °C, 60 min) result in high thermal stability (322 °C vs 218 °C), longer particle length and enhanced crystallinity (82.8% vs 77.9%) compared to H₂SO₄ hydrolyzed (64 wt.%, 45 °C, 45 min) CNCs. Luzi et al. (2019) extracted CNCs from North African grass (Diss) stems through H₂SO₄ hydrolysis upon pretreating cellulose obtained from Diss stems employing various chemical pretreatments, which are de-waxing, bleaching with NaClO₂ and treatment with NaHSO₄ and NaOH, and enzymatic pretreatment *via* xylanase, polygalacturonase and cellulase. They highlighted that chemically pretreated fibers offer CNCs with compact size, while enzymatic pretreatment resulted in CNCs with higher crystallinity and thermal stability. It has been reported that in comparison to CNF and BNC, CNCs encompass superior mechanical properties on account of their high crystallinity. Out of all the nanocellulose forms, only CNCs have been endorsed as safe by numerous standards (Yang & Cranston, 2014). Figure 2.5 depicts the mechanism of the chemical and mechanical methods to produce CNC and CNF from cellulose.

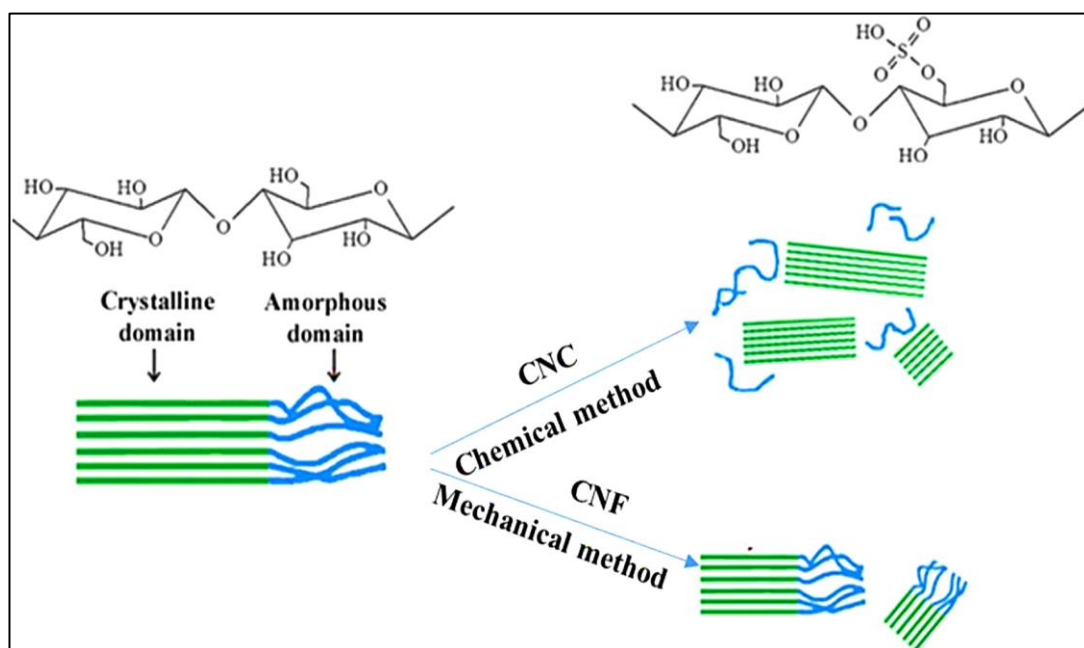


Figure 2.5: The mechanism of chemical and mechanical methods for producing CNC and CNF from cellulose (adapted from Sofla et al. (2016))

Modified CNCs were initially explored for use as reinforcing materials before they could be innovatively tested for fluorescence bioimaging applications (Li et al., 2022). Plenty of studies have explored the utility of CNCs as reinforcing materials for various applications, for instance, in gelatin hydrogels for controlled drug delivery systems (Ooi et al., 2016), chitosan films (Mujtaba et al., 2017), poly(vinyl alcohol) films (Popescu, 2017), natural rubber nanocomposites (Koeipudsa et al., 2022), cement composites (Fan et al., 2022), sodium alginate-based superabsorbent-fertilizer hydrogel (El Idrissi et al., 2022), core-shell hydrogels for sustained release of fertilizer and water retention (do Nascimento et al., 2022), bio-nanocomposite film for food packaging (Gupta et al., 2021), highly compressible hydrogel for ultrasound scanning (Cheng et al., 2022), calcium alginate hydrogels for methylene blue adsorption (Soleimani et al., 2023), spider-web-inspired membrane for oil/water separation (Q. Wang et al., 2022), photocurable thermosetting elastomer for 3D printing (Palaganas et al., 2022), and nanocomposite coating for wood furniture (Kaboarani et al., 2017).

It is interesting to note that CNCs as nanomaterials have undisputable physical and excellent biological properties that enhance their interest as biomedical materials (Aziz et al., 2021; Ganguly et al., 2020; Mali & Sherje, 2022; Sunasee et al., 2016). For instance, Long et al. (2021) developed a novel method for fabrication of CNC-based pH responsive drug delivery system for anticancer drug doxorubicin. The biological evaluation results affirmed that the developed drug carrier revealed negative